frontiers | Frontiers in Astronomy and Space Sciences

TYPE Original Research
PUBLISHED 12 March 2025
DOI 10.3389/fspas.2025.1504288

OPEN ACCESS

EDITED BY
Josep M. Trigo-Rodríguez,
Institute of Space Sciences, Spanish National Research Council (CSIC), Spain

REVIEWED BY
Akos Kereszturi,
Hungarian Academy of Sciences (MTA), Hungary
Mauro S. Ferreira Santos,
NASA Jet Propulsion Laboratory (JPL), United States

*CORRESPONDENCE
C. Gil-Lozano,
carolina.gil.lozano@uvigo.es

RECEIVED 30 September 2024
ACCEPTED 14 February 2025
PUBLISHED 12 March 2025

CITATION
Gil-Lozano C, Mateo-Martí E, Gago-Duport L, Losa-Adams E, Sampedro MF, Bishop JL, Chevrier V and Fairén AG (2025) Evaluating the reactivity of pyrite on Mars under current and ancient geochemical environments. *Front. Astron. Space Sci.* 12:1504288. doi: 10.3389/fspas.2025.1504288

Evaluating the reactivity of pyrite on Mars under current and ancient geochemical environments

C. Gil-Lozano[1]*, E. Mateo-Martí[2], L. Gago-Duport[1], E. Losa-Adams[2], M. Fernández Sampedro[2], J. L. Bishop[3], V. Chevrier[4] and A. G. Fairén[2,5]

[1]Centro de Investigación Mariñas, XM1, Universidade de Vigo, Vigo, Spain, [2]Centro de Astrobiología (CAB) CSIC-INTA, Madrid, Spain, [3]Carl Sagan Center, SETI Institute, Mountain View, CA, United States, [4]Arkansas Center for Space and Planetary Science, University of Arkansas, Fayetteville, AR, United States, [5]Department of Astronomy, Cornell University, Ithaca, NY, United States

Alteration of pyrite-bearing basalt on Mars could provide an important source of sulfates, iron oxides/hydroxides and amorphous silica. Natural semiconducting minerals can undergo photooxidation reactions under UV irradiation due to the generation of electron holes. In this work, we experimentally investigate the photocatalysis of pyrite (FeS_2)-olivine (Fo_{85}) weathered microparticles under simulated current Martian surface conditions (pCO_2 ~ 7 mbar, UV (200–400 nm) flux ~ 2.3 W/m^2). Our results demonstrate that chemical reactions under current Mars-like conditions facilitate hydration and transfer redox reactions of natural semiconducting minerals, driving the rapid formation of sulfates, iron oxides and amorphous silica within 72 h. These results highlight the role of natural semiconducting minerals in weathering processes under present-day Martian conditions. In addition, we performed geochemical simulations to evaluate the formation pathway of secondary minerals resulting from the weathering of pyrite-rich and pyrite-free basalt substrates during a transient warm episode on a generally cold and wet early Mars. Our models account for the contribution of oxidants to the Martian regolith via the spontaneous production of H_2O_2 in bulk water during the aqueous dissolution of pyrite microparticles. The models show differences in the types of secondary byproducts with sulfate and iron-oxide formation from pyrite weathering, especially during the cooling periods when gypsum formation increased significantly.

KEYWORDS

martian climate, weathering, photocatalysis, pyrite, olivine, mineralogy

1 Introduction

The surface of Mars, which lost most of its atmosphere to space between 4.2 and 3.5 Gyr ago (Jakosky et al., 2018), receives high levels of ultraviolet radiation (UV). Previous studies of photochemical reactions on the Martian surface have mainly focused on how organic compounds can be shielded by mineral matrices (Carrier et al., 2019) and on the formation of strongly oxidizing agents such as perchlorate (Schuttlefield et al., 2011). However, little attention has been paid to the UV-induced redox chemistry of semiconducting minerals and

its effect on surrounding minerals on a planet where natural photochemical transformations could have occurred over long periods of time.

Natural minerals are excellent photocatalysts and have been widely used in advanced oxidation processes to remove organic pollutants from water because of their large surface areas and high adsorption capacities (Tang et al., 2022; Gil-Lozano et al., 2014). These include pyrite, a disulfide mineral with a suitable band gap (E.g., = 0.95eV) and high surface reactivity (Herbert et al., 2013; Galvez-Martinez et al., 2019). Previous work has demonstrated the photocatalytic ability of this semiconducting mineral to facilitate N_2 fixation under Mars-simulated surface conditions (Mateo-Marti et al., 2019). However, its photo-oxidative power in a matrix with silicate primary minerals such as olivine, which is very sensitive to surface reactions, is an unexplored alteration process that may be relevant to Mars' geologically recent past.

Although, large scale deposits of sulfide minerals have not been reported on the surface of Mars, Burns (Burns, 1988; Burns, 1993) proposed aqueous alteration of basaltic rocks containing Fe-rich olivine and sulfides, including pyrite, to form assemblages of sulfates, clays, and iron oxide/oxyhydroxides on the surface of Mars. In fact, the Martian mantle is thought to contain more sulfur than Earth's mantle (Gaillard and Scaillet, 2009), and data from Martian meteorites suggest that the primary sulfur mineralogy is dominated by sulfide minerals (Franz et al., 2019; Chevrier et al., 2011; Lorand et al., 2018). In addition, pyrite has been identified in Martian regolith breccias NWA7533 and 7455 (Lorand et al., 2015; Wittmann et al., 2015), and has been detected *in situ* by the Mars Science Laboratory (MSL) at Gale Crater: in Yellowknife Bay (Vaniman et al., 2014), the Rocknest deposit (McAdam et al., 2014), and the Glent Torridon region (Wong et al., 2022). Investigation of aqueous alteration of volcanic material on Hawaii and Iceland indicates that low-temperature (<100°C) alteration of pyrite could be contributing greatly to the S cycle and production of sulfates on Mars (Moore and Szynkiewicz, 2023). Furthermore, sulfate formation via heterogeneous pathways involving volcanic SO_2 emissions and interfacial water layers highlights additional processes that could contribute to sulfate distribution under current surface conditions on Mars (Góbi and Kereszturi, 2019).

Looking back at the aqueous geochemical history of the planet, sulfide weathering has also been considered an important mechanism of sulfate and iron oxy (hydroxide) formation at several locations on the surface of Mars, such as the sulfate veins (Schwenzer et al., 2016) or the akaganeite deposits (Peretyazhko et al., 2021) at Gale Crater, the sulfate- and phyllosilicate-bearing sedimentary rocks at Meridiani Planum (Zolotov and Mironenko, 2016), or the alunite-bearing deposit at Cross Crater (Ehlmann et al., 2016). Previous experimental studies have shown that the oxidative weathering of pyrrhotite (Chevrier et al., 2006; Chevrier et al., 2004), as well as pyrrhotite-silicate mixtures under a CO_2 atmosphere (Dehouck et al., 2012; Dehouck et al., 2016), and the weathering of pyrite and pyrrhotite after exposure to highly oxidizing Cl and Br fluids (Mitra et al., 2023), can lead to the formation of abundant sulfate and oxidized iron minerals. However, the ability of pyrite microparticles to spontaneously generate hydrogen peroxide (H_2O_2) and other reactive oxygen species (ROS) during their aqueous dissolution (Borda et al., 2001; Javadi Nooshabadi and Hanumantha Rao, 2014; Gil-Lozano et al., 2017) is a reaction mechanism that has never been tested in an ancient aqueous Mars geochemical environment under a thicker CO_2-rich atmosphere, where O_2 does not appear to have been a major oxidant. While oxidation reactions under anoxic conditions induced by mineral surfaces have been well documented in the laboratory, their importance in natural environments has only recently been demonstrated with the formation of O_2 under anoxic conditions on the ocean floor associated with polymetallic nodules (Sweetman et al., 2024). This finding could have significant implications for the geochemical evolution of Earth's atmosphere and the development of life, and it may also have been of similar importance on ancient Mars.

In the present study, we first experimentally investigate the photocatalysis of an initially weathered sample composed of FeS_2-Fo_{85} microparticles after 72 h of irradiation under simulated present-day Martian surface conditions (CO_2 pressure pCO_2 ~ 7 mbar, UV (200–400 nm) flux ~ 2.3 W/m^2). Our aim in this first part of the study is to analyze the evolution of the oxidized layer and its effect on the paired silicate mineral. In a second part of the study, we theoretically simulate the weathering of a pyrite-rich, pyrite-free basaltic soil in an early Martian environment. Our goal in this modeling component is to investigate the oxidation mechanism triggered by the spontaneous production of H_2O_2 during pyrite dissolution and its effect on secondary mineral formation.

2 Experimental

2.1 Samples and experimental procedure

Olivine and igneous pyrite samples were collected from the island of Lanzarote, Spain. The samples were crushed and dry sieved to a particle size of less than 20 microns to increase the surface area of the grains. X-ray diffraction patterns showed that the olivine -rich sample (Fo_{85}) also contains enstatite and diopside, whereas no other mineral was identified in the pyrite sample (Supplementary Figure S1). Powder samples were cleaned using a stepwise procedure consisting of sonication followed by centrifugation. First, the samples were sonicated in ethanol to remove organic contaminants, followed by hydrochloric acid (HCl, 0.1N) to dissolve surface oxides. Finally, the samples were washed twice in deoxygenated deionized water (Milli-Q, N_2-purged) to ensure the removal of residual impurities. The FeS_2-Fo_{85} pairing sample was prepared by weight (60 wt% pyrite and 40 wt% olivine). Despite recent advances in the field of Martian simulants preparations (Ramkissoon et al., 2019), a simplified mixture of olivine and a high amount of pyrite was intentionally used to clearly identify surface alteration within the time scale of laboratory experiments. The selection of olivine as an accessory mineral was based on its rapid weathering behaviour and the development of an SiO_2-rich alteration layer during the initial stages of alteration (Delvigne et al., 1979). The sample was then exposed to anoxic water (Milli-Q, N_2-purged) at a fluid to rock ratio in mass units of ~10 g H_2O/1 g mineral mixture (olivine + pyrite) under CO_2 atmosphere (pCO_2 = 0.5 bar) to simulate a thicker and anoxic early Martian atmosphere (Supplementary Figure S2A). Visible light was included to accelerate the dissolution of pyrite (Schoonen et al., 2000). The duration of aqueous weathering (42 days) was based on previous

studies that observed surface mineral alteration within this time lapse (Dehouck et al., 2014; Gil-Lozano et al., 2017). The sample was then dried for 5 days under the same CO_2 atmospheric conditions using silica gel as a desiccant (room temperature) to ensure removal of excess water that was not chemically or physically adsorbed.

The exposure of the dried weathered sample to UV-like Martian surface conditions was performed inside the Planetary Atmospheres Surfaces Chamber (PASC) at the Centro de Astrobiologia (CAB) (Mateo-Martí et al., 2006) (Supplementary Figure S2B). The simulated Martian atmosphere is composed of pCO_2 = 7 mbar. To achieve this controlled atmosphere, the chamber was first pumped down to a vacuum conditions of about 1×10^{-6} mbar (high vacuum) to reduce contamination from O_2 or other gases inside the chamber. CO_2 gas (Alphagaz bottle: CO_2 ~99.7 %v/v, $H_2O \leq 200$ ppm, $O_2 < 25$ ppm) was then introduced to raise the pressure from 1×10^{-6} mbar–7 mbar. A constant temperature of 295 K was used to accelerate the alteration process. The FeS_2-Fo_{85} weathered sample was irradiated with a UV deuterium lamp for a total of 72 h. This duration was chosen based on previous work confirming that clean single-crystal pyrite exhibits measurable photoreactivity within a few hours under similar conditions (Mateo-Marti et al., 2019). The UV source emits a continuous spectrum in the 200–400 nm range, which is representative of the UV radiation reaching the Martian surface (Patel et al., 2004). The source has a dose emission of 2.3 W/m^2, corresponding to F = 2.3×10^{14} (6 eV photons) cm^{-2} s^{-1} (Caro et al., 2006). This emission is about 10 times lower than the UV flux measured by the REMS instrument onboard the Curiosity Rover (Gómez-Elvira et al., 2014).

2.2 Analytical techniques

Powder X-ray Diffraction (PXRD) analyses were performed to determine the presence of accessory minerals in the initial samples. No new mineral phases were identified by XRD, as the alteration of the sample was not sufficient to be detected by this bulk technique. PXRD was performed using a Seifert 3003 TT with Cu Kα radiation (λ = 1.542 Å). The X-ray generator was set to an acceleration voltage of 40 kV and a filament current of 40 mA. The samples were scanned between 5° and 60° (2θ) with a step size of 0.05° (2θ) and a count time of 2 s per step. Qualitative analysis of the XRD patterns was performed with QualX2 software using the PDF-2 database (ICDD), while Rietveld analyses were performed with the Fullprof software (Roisnel and Rodriguez-Carvajal, 2001). A scanning electron microscope (SEM), JEOL JSM-5600 LV, equipped with an energy dispersive X-ray spectroscopy (EDX) INCA detector (20 kV) was used to characterize the morphology and chemical composition of the samples after exposure to the simulated Martian conditions.

Surface analyses were performed using Fourier transform infrared spectroscopy (FTIR) and X-ray photoelectron spectroscopy (XPS). Infrared spectra of the mineral samples were analyzed using the diffuse reflectance technique (DRIFT) with a Nicolet FTIR spectrometer. Spectra were collected using a DTGS-KBr detector with 2 cm^{-1} resolution in the mid-infrared region (from 4,000 to 400 cm^{-1}) with an XT-KBr beamsplitter. Each spectrum is an average of three independent measurements (64 scans, 2 cm^{-1} resolution). XPS analyses of the samples were performed in an ultrahigh vacuum chamber equipped with a hemispherical electron analyzer (Phoibos 150 MCD) and an Al Kα X-ray source (1,486.7 eV) with an aperture of 7 × 20 mm. The base pressure in the ultra-high vacuum chamber was 1×10^{-8} mbar and the experiment was performed at room temperature. A 30 eV pass energy was used for the acquisition of the overview sample, while a 20 eV pass energy was used for the analysis of the following core-level spectra: O 1s, C 1s, N 1s, Fe 2p, S 2p and Si 2p. The XPS spectra regions were fitted and deconvoluted using the CasaXPS software (Fairley et al., 2021).

2.3 Geochemical modeling

The geochemical simulations were performed with the PHREEQCI 3.7.3 speciation-reaction code (Parkhurst and Appelo, 2013) using the Lawrence Livermore National Laboratory (LLNL) thermodynamic database. This database was modified to include thermodynamic data for a variety of smectite and zeolite minerals from the Thermoddem database, the kinetic rate constants for mineral dissolution and precipitation (Zhang et al., 2019), and a kinetic expression for the formation of H_2O_2 during pyrite dissolution (see Supplementary Appendix 1 in the Supplementary Material for script example).

The goal of the models is to analyze the secondary mineral formation pathways resulting from the weathering of a pyrite-rich and a pyrite-free basalt substrate under the same environmental conditions. In particular, the geochemical scenario simulates the water-rock reaction of a stagnant surface water in equilibrium with an anoxic CO_2-rich atmosphere (Supplementary Figure S3). After 150 years, this system simultaneously loses pCO_2 and cools, representing a transitional warm event in a generally cold and wet early Martian environment (Bishop et al., 2018; Fairén, 2010; Feldman et al., 2024).

The compositions of the pyrite-rich and pyrite-free basalt substrates used in the models are described in Table 1. An olivine-rich basalt composition was intentionally used to have a quick source of iron when modeling the pyrite-free basalt scenario. In each run, a pyrite-rich or pyrite-free basalt substrate was reacted with an initial solution of pure water equilibrated with a CO_2 atmosphere (pCO_2 = 0.5 bar, T = 20°C). The models consider the same set of potential secondary minerals (Supplementary Table S1) that could be formed and redissolved during the simulation time (up to 300 years). The list of secondary minerals includes phyllosilicates, sulfates, oxides, carbonates, and zeolites that are representative of the mineral alteration observed on the Martian surface. In the models, therefore, the amount of mineral reacting with the solution is controlled by the dissolution rate, which depends on the surface area (A_0/V surface area of mineral per unit water mass) of the primary minerals (Fairén et al., 2017). Kinetic rates were modeled using the kinetic script library developed by Zhang et al. (2019) based on the transition state theory rate law (Lasaga, 1998; Palandri and Kharaka, 2004). In particular, the kinetic rate law of pyrite is catalyzed by the presence of H_2O_2, Fe^{3+}, and O_2 (McKibben and Barnes, 1986). In the simulations, the primary oxidant is the H_2O_2 formed on the reactive surface of pyrite, simulating an autocatalytic process. The formation of H_2O_2 at the pyrite surface was modeled using a kinetic expression that relates the number of defects undergoing oxidation to the

TABLE 1 Substrate composition used in the models.

	Pyrite-rich basalt substrate			Pyrite-free basalt substrate		
	vol%	Initial moles (mol/kgw)	*Surface area (m^2/kgw)	vol%	Initial moles (mol/kgw)	*Surface area (m^2/kgw)
Anorthite	15	4.051	0.245	20	5.401	0.327
Albite	11.25	3.204	0.192	15	4.273	0.256
Sanidine	3.75	1.009	0.066	5	1.346	0.088
Diopside	11.25	3.892	0.149	15	5.189	0.198
Enstatite	18.75	6.996	0.263	25	9.328	0.351
Olivine	15	7.988	0.206	20	10.650	0.275
Pyrite	25	15.611	0.224	0	0.000	0.000

(*) The surface area was estimated using a geometric model approach, considering the mass fraction of each mineral, a porosity of 0.3, and assuming spherical grains (radius = 0.5 mm). Finally, the estimated values were reduced by an order of magnitude to account for the effective fraction of the surface that is reactive (Sonnenthal et al., 2005).

surface area of pyrite. This model predicts that H_2O_2 is continuously introduced into the system as long as pyrite dissolution proceeds (see Supplementary Appendix 1 in the Supplementary Material).

3 Results

3.1 Experimental results: present-day Mars conditions

We studied the photocatalysis of a mixture of FeS_2-Fo_{85} microparticles after exposure to present-day Martian surface conditions (pCO_2 ~ 7 mbar, UV (200–400 nm) flux ~ 2.3 W/m^2). The initial sample was previously altered in water equilibrated with a CO_2-rich atmosphere (pCO_2 = 0.5 bar, W/R ~ 10 wt%) and then evaporated under the same atmosphere. This process simulates a warmer period of early Mars and aims to evaluate the effect of a partially oxidized surface layer on the photocatalytic properties of the disulfide-silicate mixture.

Figure 1 shows the DRIFT spectra, where we can distinguish surface alteration by-products characterized by the presence of several bands in the region of 2,300–750 cm^{-1}, related to the asymmetric and symmetric stretching vibrations of Si-O (from olivine and amorphous silica) and S-O (from sulfoxyanions), as well as their corresponding bending vibrations in the region below 750 cm^{-1} (Lane, 2007; Ellerbrock et al., 2022). The specific band assignments in these regions are complex due to the strong band overlap caused by the coexistence of different chemical groups (e.g., polysulfides, sulfite, sulfate, silicate, amorphous silica) in different chemical environments (e.g., bridging, outer, inner sphere) (Peak et al., 1999). Overall, after exposure to current Martian surface conditions, the sample showed a decrease in disulfide (S-S) stretching at 435 cm^{-1} and an increase in stretching (3,800–2,800 cm^{-1}) and bending (1700–1,600 cm^{-1}) modes of H_2O. In addition, the bands at 1,145 and 1,102 cm^{-1} showed a significant increase. We tentatively attribute the band at 1,145 cm^{-1} to an increase in sulfate, likely in a chemical environment similar to that of gypsum, with reduced distortion of the v_3 band, resulting in the predominance of a single band (Lane, 2007). Additionally, the band at 1,100 cm^{-1} is assigned to an enhancement of the amorphous silica coating (Ellerbrock et al., 2022). The increase in hydration of this sample also supports the increase in hygroscopic by-products such as silica and sulfate. Interestingly, we also observed changes in the v_3 stretching region of carbonates (i.e., 1,275–1,590 cm^{-1}) (Bishop et al., 2021). The initial weathered sample showed a band at 1,425 cm^{-1}, assigned to calcite. However, after exposure to Mars' surface conditions, this band split into three bands, indicating a symmetry reduction of the carbonate compound (Bishop et al., 2021).

Using XPS, we further analyzed the evolution of the surface alteration layer after exposure to current Mars-like surface conditions. Quantification of the XPS survey spectra showed a significant increase in the oxygen contribution after exposure to current Martian surface conditions (Supplementary Figure S4), which is consistent with the increase in silica, sulfate, and the increase of the hydration level found in the DRIFT spectra. The most notable changes related to pyrite alteration occurred in the Fe $2p_{3/2}$ and S $2p_{3/2}$ orbitals, where surface species shifted towards higher values of binding energies. This is associated with an increase in the oxidation state of the corresponding species (Schaufuß et al., 1998). Considering that high-spin Fe(II) and Fe(III) compounds give rise to multiplet splitting and satellite features (Grosvenor et al., 2004), the fitting of Fe 2p in chemical environments of different iron species (such as sulfates, oxides and oxyhydroxides) is challenging due to peak overlap. Nevertheless, the shape of the Fe 2p spectra showed significant differences before and after exposure to Martian surface conditions (Figure 2). The initial weathered sample showed a well resolved peak assigned to the Fe-S contribution of pyrite (Fe $2p_{3/2}$ ~ 707.6 eV) and a broad tail towards higher binding energies, indicating the presence of Fe(II) and possibly some Fe(III) compounds. However, after simulating Martian surface conditions, the Fe-S peak showed a significant decrease while the asymmetric tail increased at higher binding energies, consistent

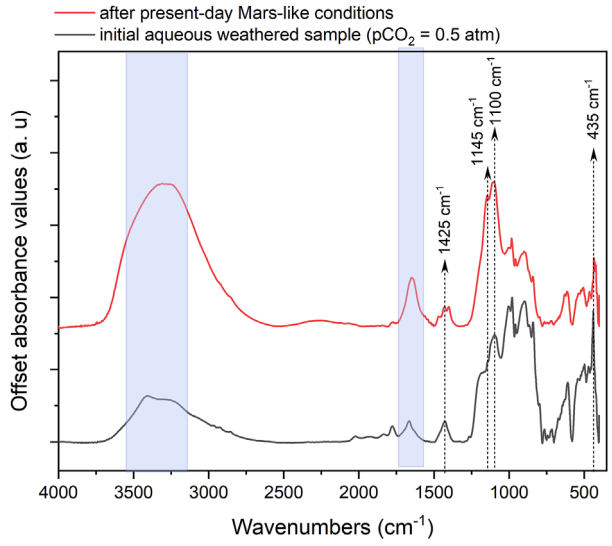

FIGURE 1
DRIFT spectra showing the initial weathered sample prior to exposure to Martian surface conditions at the bottom and after exposure to Martian surface conditions at the top. The arrows mark the asymmetric stretching mode of carbonate (1,425 cm^{-1}), sulfate (1,145 cm^{-1}), and amorphous silica (1,102 cm^{-1}) and the disulfide bond in the pyrite lattice (435 cm^{-1}). The shaded area indicates the frequency range of the H_2O stretching and bending vibrational modes.

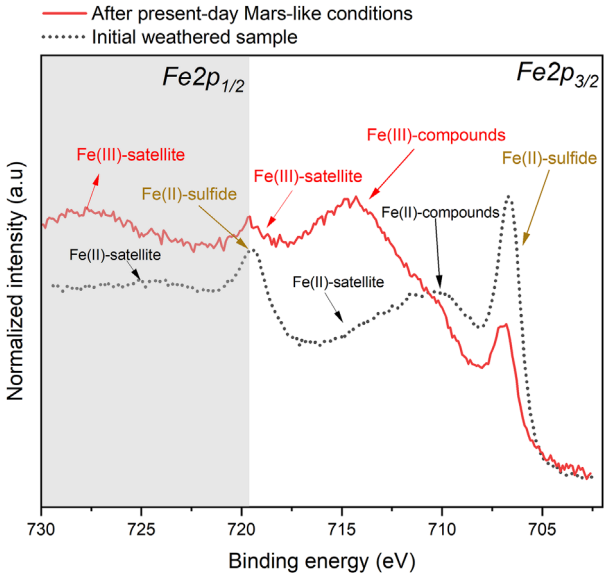

FIGURE 2
Fe 2p orbital of the FeS_2-Fo_{85} pairing sample before (dotted line) and after (solid line) exposure to present-day Martian surface conditions. The labels in the figure show the location (binding energy) of the major contribution of the iron species along with its satellite peaks. The spectra were normalized using Min-Max normalization method.

with an increase in Fe(III) compounds. This is further supported by the appearance of Fe(III) satellite peaks (Grosvenor et al., 2004). Figure 3A illustrates the fitting of the S 2p spectra. We identified three spin-orbit components, assigned to S_2^{2-} (S $2p_{3/2}$ 162.1 ± 0.1eV), S_n^{2} (S $2p_{3/2}$ 164.2 ± 0.1eV), SO_3 (S $2p_{3/2}$ 166.7 ± 0.1eV) and SO_4^{2-} (S $2p_{3/2}$ 169.5 ± 0.1eV), respectively. Following exposure to Martian surface conditions, the sample exhibited a notable increase in sulfate contributions, accompanied by the emergence of a new peak at the highest binding energy (172.5 eV). This peak can be attributed to the emergence of a ferric hydroxysulfate compound (Todd et al., 2003), possibly due to hydroxylation at pyrite defect sites (Xian et al., 2019), along with an increase in the Si 2s plasmon, which is also observed in the Si 2p plasmon. Overall, the Fe 2p and S 2p spectra showed a decrease in iron disulfide species in favor of iron sulfate and iron oxide/oxyhydroxide formation.

Similarly, we observed a significant change in the Si 2p spectra (Figure 3B). The initial weathered sample showed the major peak at 102.5 ± 0.1 eV, assigned to silicate. After exposure to Martian surface conditions, this contribution decreased, while the peak at 105.1 ± 0.1 eV, assigned to hydroxylated silica, increased (Kwak et al., 2011). The O 1s spectra of the sample after exposure to current Martian surface conditions also shifted to higher binding energies, which is related to the increased OH and H_2O species on the surface of the sample (Supplementary Figure S5). Unfortunately, the coexistence of various compounds within the narrow binding energy range of the O 1s orbital makes accurate deconvolution challenging. These findings are further corroborated by EDX analysis, which revealed an oxygen enrichment in olivine particles after exposure to current Martian surface conditions (Supplementary Figure S6).

3.2 Model results: early Mars conditions

The geochemical simulations represent ponded water in equilibrium with a CO_2 atmosphere undergoing progressive cooling and pCO_2 reduction (Fairén et al., 2009; Fairén et al., 2011) (Supplementary Figure S3). The boundary conditions, including the primary mineral assemblage and the list of secondary minerals that could form, are the same in both simulations except for the presence of pyrite in one of them (Table 1; Supplementary Table S2). Therefore, the model results allowed us to specifically evaluate the effect of H_2O_2 production from pyrite dissolution on the secondary minerals formed.

As expected, the pH evolution is strongly dependent on pCO_2 variations in the atmosphere, regulated by the CO_2-bicarbonate-carbonate buffering system (Figure 4). In both simulations, the pH of the initial solution is acidic (pH_0 ~ 4) but rises rapidly due to chemical weathering of silicate until it reaches a pH close to 6.4, which allows carbonate precipitation and buffers the pH. However, in the pyrite-rich substrate, the pH buffering value is slightly lower, around 6.2, and when pCO_2 is reduced (in the cooling phase), the increase of the pH is less pronounced due to the acidic dissolution of pyrite.

It is noteworthy that in the simulation with the pyrite-rich substrate, the formation of siderite (iron carbonate) is inhibited, despite the iron supply by the pyrite dissolution. This is due to the oxidizing conditions that favor instead the formation of hematite (Fe(III) iron oxide) (Baron et al., 2019), which is kept stable during the whole simulation (warm and cold periods), while nontronite (Fe(III)-rich clay) is only formed in the cooling period. In the pyrite-free scenario, however, hematite (followed by nontronite) is only formed in the cooling period, when basalt dissolution slows down

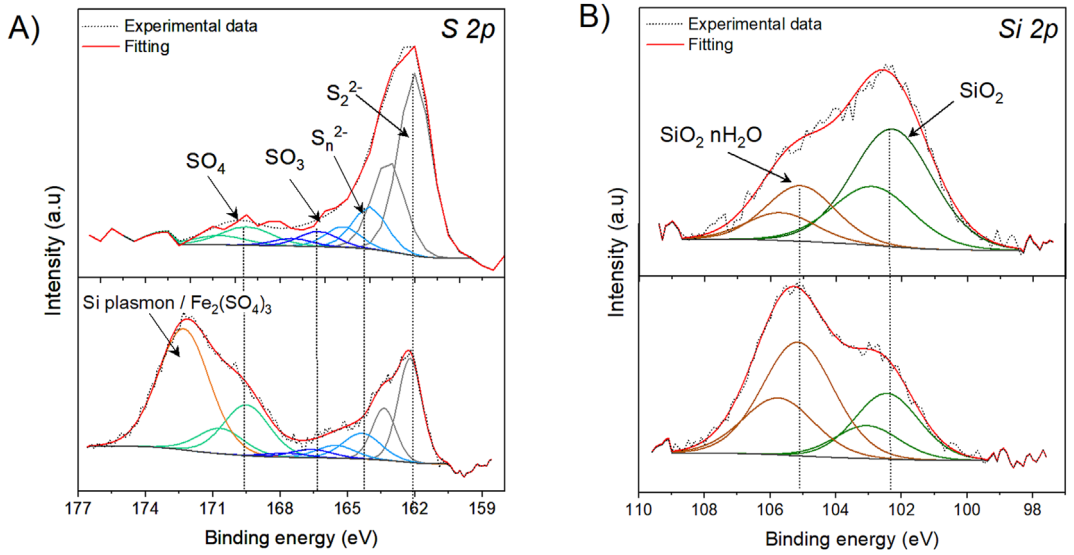

FIGURE 3
Curve fitting XPS spectra of the **(A)** S 2p orbital and, **(B)** Si 2p orbital. The initial weathered sample, before being exposed to Martian surface conditions, is shown at the top, and after having been exposed to Martian surface conditions at the bottom. Dotted lines mark the binding energy of the S **(A)** and Si **(B)** species identified in the analysis.

and Eh gradually increases. Interestingly, this increase in Eh causes the destabilization of siderite, which begins to dissolve at the end of the simulation. Consequently, Fe^{2+} is released into the solution, lowering the redox conditions again and favoring the formation of magnetite (Fe(II)Fe(III) iron oxide).

Since Ca-plagioclase (anorthite) is a major component of the substrate and dissolves quickly under these geochemical conditions, kaolinite and montmorillonite are the most abundant clay minerals formed in both simulations.

In the pyrite-rich substrate, we also observe the formation of sulfates due to the higher oxidation of the iron sulfide. The first sulfate to precipitate is alunite, a common weathering product of pyrite dissolution. It begins to form in year 29 and remains stable until year 257, when it is dissolved by the increase in pH that favors the formation of zeolite (Ca-heulandite). Gypsum, which is more soluble, begins to form in year 115 and remains stable since then. Interestingly, at the end of the simulation gypsum experienced a rapid increase coinciding with the start of calcite dissolution, which releases Ca^{2+} into the solution.

These results revealed the strong competition between minerals for the available cations throughout the whole simulation time (Fairén et al., 2017). Overall, the main difference between both simulations shows that dissolution of the pyrite-rich basalt substrate induces higher redox conditions favoring the formation of ferric-bearing minerals and sulfates even in a CO_2 rich anoxic atmosphere.

4 Discussion

We experimentally studied the photocatalysis of a disulfide mineral associated with olivine under current Mars-like surface conditions (pCO_2 = 7 mbar, UV flux ~2.3 10^{14} cm^{-2} s^{-1}). Our initial weathered sample showed an increase of the oxidation layer after a short reaction time of 72 h. This indicates that the photoactivation of the sample is not hindered by the surface coating of the initially weathered sample. In fact, previous research has demonstrated that pyrite surface oxidation can create a natural (hydr)oxide-pyrite photoelectrochemical tandem cell, which enhances its ability to induce water oxidation (Eggleston et al., 2012).

After UV-like Mars surface alteration, the sample showed the emergence and increase of IR bands related to the sulfate and silica stretching vibrations (Figure 1) (Lane, 2007; Ellerbrock et al., 2022). This was accompanied by an increase in the degree of hydration, consistent with the formation of hygroscopic by-products such as silica and sulfate on the surface of the sample. The most superficial XPS analysis also supported the increase in the oxygen content of the sample (Supplementary Figure S4), and the enhancement of the degree of oxidation due to the rise in ferric oxides and sulfate species assigned in the high-resolution XPS spectra (Figures 2, 3). Therefore, according to our experiments, UV photoactivation of pyrite makes it highly reactive under current Martian surface conditions. This helps to explain the absence of large sulfide deposits on the Martian surface to date, as they are likely obscured by a coating of secondary products (e.g., oxides, sulfates, and hydrated silica). However, volcanogenic massive sulfides (VMS), similar to those driving the geochemical conditions found at Rio Tinto (Amils et al., 2007), could exist in the Martian subsurface (Burns and Fisher, 1990). Previous estimates of the sulfur budget, based on meteorite data and fractional crystallization models of magmas, suggest that a substantial amount of sulfur could be sequestered in deep crustal sulfide-rich deposits (Ding et al., 2014). Internal layered deposits associated with the Valles Marineris chasma system could potentially be explained by groundwater circulation through these sulfide-rich deposits (Bishop et al., 2009).

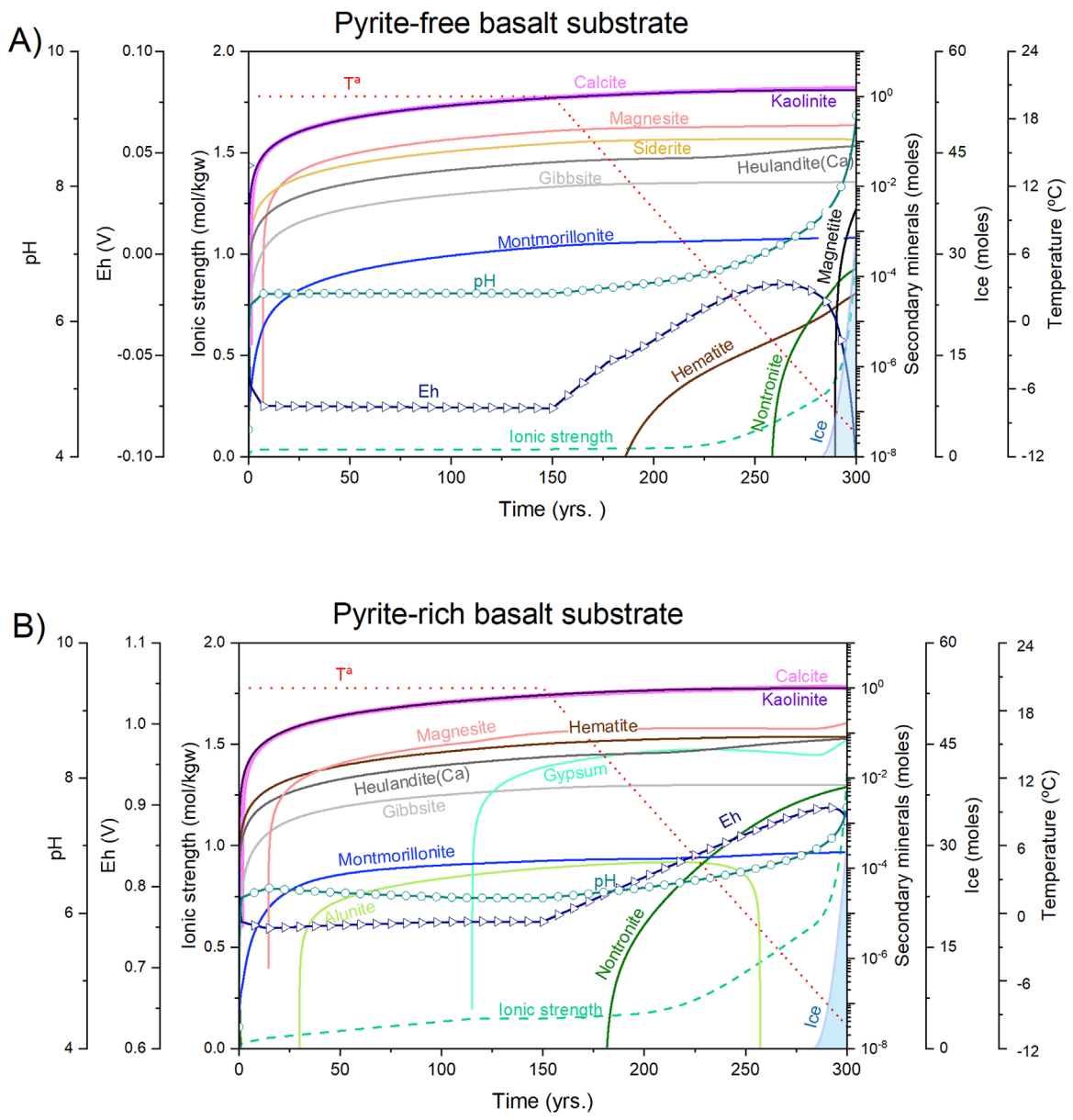

FIGURE 4
Model results showing the formation of by-products over time from the weathering of a pyrite-free **(A)** and pyrite-rich **(B)** basalt substrate. The solution is equilibrated with an atmosphere of CO_2 (pCO_2 = 0.5 bar), which has been subjected to a cooling period and a pCO_2 reduction.

A significant shift of the silicate component to higher binding energies is observed in the Si 2p spectra (Figure 3B), which is related to the formation of a hydroxylated silica layer (Kwak et al., 2011). This observation aligns with the growth of amorphous silica identified in the FTIR spectra and the increased oxygen contribution detected by XPS and EDS analyses (Figure 2; Supplementary Figures S4, 5). Several studies have shown that natural mineral composites can enhance the photocatalytic efficiency of semiconductors by increasing electron charge mobility and/or reducing electron-hole recombination (e.g., Tang et al., 2022). In particular, diatomite, which is mainly composed of amorphous SiO_2, has been widely used as a charge carrier due to its high porosity, large specific surface area, and strong chemical stability (Zhu et al., 2018). Consequently, the formation of a hydrated silica layer on the sample may provide more active sites for adsorption and facilitate the mobility of electrons and holes induced by the photoactivation of pyrite (Supplementary Figure S7). These results indicate the need for further research on the photocatalytic role of altered olivine, as well as the susceptibility of more representative iron-rich Martian simulants to UV photo-oxidation.

Interestingly, we also detected changes in the stretching modes associated with carbonates (Figure 1). The band at 1,425 cm^{-1}, assigned to calcite, split into three components. This band splitting suggests a change in the symmetry and/or crystallinity of the carbonate compound (Bishop et al., 2021; Gago-Duport et al., 2008). The instability of carbonates under UV irradiation was investigated

by (Mukhin et al., 1996). However, later studies showed that carbonates cannot be photodegraded by the UV flux incident on the Martian surface (Quinn et al., 2006). Our experiments suggest that the photocatalysis of pyrite-silicate composites may induce changes in the crystallinity of the carbonate film.

Another interesting aspect of pyrite surface reactivity is its ability to spontaneously produce H_2O_2 and ROS during this aqueous dissolution (Borda et al., 2001; Javadi Nooshabadi and Hanumantha Rao, 2014; Wang et al., 2012). In fact, aqueous dissolution of mechanically active pyrite microparticles has been shown to generate H_2O_2 even in oxygen-limited environments (Gil-Lozano et al., 2017; Zhang et al., 2016). H_2O_2 is an oxidant already identified in the Martian atmosphere (Clancy et al., 2004) and a potential oxidant of the Martian regolith (Chevrier et al., 2006; Lasne et al., 2016). Oxidative weathering of sulfide minerals has been suggested as an important diagenetic mechanism on early Mars for sulfate production (Wong et al., 2022; Dehouck et al., 2016; Burns and Fisher, 1990; Rampe et al., 2020) and even as an energy source for chemolithotrophic microorganisms (Macey et al., 2020).

In the second part of this study, we modeled the ability of aqueous pyrite dissolution to generate H_2O_2 and ROS in an early wet Martian environment. Our goal is to explore differences in secondary mineralogy as a function of the disulfide content in the substrate. Therefore, models simulated the weathering of pyrite-rich and pyrite-free basalt substrates under a CO_2 atmosphere in a transient warm episode (T^a = 20°C) in a generally cold and wet Early Mars (Bishop et al., 2018; Fairén, 2010) (Supplementary Figure S3). The secondary minerals formed on the pyrite-rich substrate show a higher amount of ferric-bearing minerals (including hematite, nontronite) (Figure 4). On the pyrite-free basalt substrate, the iron is mainly sequestered in siderite, although some amounts of hematite, nontronite and magnetite were also formed during the final stage of the cooling period (Figure 4B). Similar changes in redox mineral assemblages have been recorded in various sedimentary units at Gale Crater, including Yellowknife Bay and the Murray Formation, or Glen Torridon and the Vera Rubin Ridge region. In addition, all samples analyzed by the Curiosity Rover at Gale Crater revealed the presence of volatiles (S and Cl) in X-ray amorphous phases, some of which may originate from altering sulfates (David et al., 2022). Indeed, several authors have hypothesized that influxes of groundwater fluids generated by oxidative weathering of sulfides may have driven these changes (Schwenzer et al., 2016; Peretyazhko et al., 2021; Rampe et al., 2020).

It is noteworthy that carbonates are formed in abundance in our models, while only small amounts of siderite were recorded at Gale crater (Thorpe et al., 2022). This could be explained by the fact that we did not consider a nucleation barrier for carbonate formation (Jiang and Tosca, 2020), together with the olivine-rich substrate composition used in the models, which favors carbonate formation (i.e., olivine ≥15% Vol, Table 1) (Gil-Lozano et al., 2024). The weathering of the pyrite-rich substrate also showed the formation of sulfates, gypsum being the most abundant. This is because the pH of the solution is not acidic enough to favor the formation of more acidic sulfates (e.g., jarosite). Therefore, the mobilization of these pyrite-rich weathering fluids could explain formation of the calcium sulfate veins identified at Gale Crater (Nachon et al., 2014). Furthermore, the paragenesis of phyllosilicates and sulfates identified at different locations on Mars, such as Columbus Crater (Wray et al., 2011), Cross Crater (Ehlmann et al., 2016), Mawrth Vallis (Wray et al., 2010), Noctis Labyrinthus (Weitz et al., 2011) can be alternatively explained by the weathering of pyrite-rich substrates instead of by highly acidic conditions driven by SO_2 volcanism.

In summary, the modeling results indicate that self-generated H_2O_2 from pyrite dissolution in an O_2-limited and CO_2-rich atmosphere can produce sufficient oxidation to form ferric minerals and sulfates.

Similarly, previous studies have identified sulfide minerals in SNC meteorites (shergottites, nakhlites, and chassignites) of both magmatic (Chevrier et al., 2011) and hydrothermal origin (Lorand et al., 2015). The oxidation potential of pyrite assessed in this study is consistent with the presence of Fe-oxides associated with pyrite in the NWA 7533 meteorite (Hewins et al., 2017), the sulfate phases likely formed on Mars in the MIL 03346 meteorite (McCubbin et al., 2009), and the observed relationships between sulfide and sulfate in basaltic shergottites (Shidare et al., 2021). These results support the hypothesis that pyrite, through its oxidative dissolution, could play a key role in the sulfur cycle on Mars. However, the high diversity associated with sulfate-rich deposits suggests the interplay of multiple mechanisms, including aqueous alteration, sulfide oxidation, and UV-driven photochemistry, in sulfur transformation on Mars (Changela et al., 2022).

5 Conclusion

We investigated the photocatalysis of a partially altered disulfide-olivine pairing sample under current Martian surface conditions. Our experimental results showed a high degree of oxidation in short reaction times with the growth of iron oxides, sulfates, and an amorphous silica layer. These results highlight the important role that natural semiconducting minerals can play in driving redox reactions in the recent past of Mars.

Furthermore, we modeled the ability of aqueous pyrite dissolution to generate H_2O_2 and trigger the oxidative weathering of a pyrite-rich basaltic substrate in an anoxic CO_2-atmosphere on early Mars. Our modeling results indicate different redox mineral assemblages for a pyrite-rich and a pyrite-free basalt substrate, indicating the formation of ferric iron oxides and sulfates from the pyrite-rich substrate. In addition, these redox gradients are of significant astrobiological importance because of their fundamental role in sustaining life, and may help explain the formation of intriguing rocks such as 'Cheyava Falls', discovered by NASA's Perseverance rover, We conclude, the reactivity of pyrite to ferric oxides and sulfate minerals under both present-day and early Martian surface conditions could explain the scarcity of disulfide deposits on the Martian surface to date.

Data availability statement

The original contributions presented in the study are included in the article/Supplementary Material, further inquiries can be directed to the corresponding author.

Author contributions

CG-L: Conceptualization, Formal Analysis, Methodology, Writing–original draft. EM-M: Formal Analysis, Methodology, Writing–review and editing. LG-D: Conceptualization, Formal Analysis, Writing–review and editing. EL-A: Writing–review and editing. MS: Formal Analysis, Writing–review and editing. JB: Writing–review and editing. VC: Writing–review and editing. AF: Conceptualization, Supervision, Writing–review and editing.

Funding

The author(s) declare that financial support was received for the research, authorship, and/or publication of this article. "SOS-Mars" PID2020-119412RJ-I00 of the Spanish Ministry of Science and Innovation "MarsFirstWater" (Consolidator Grant no. 818602), funded by the European Research Council.

Acknowledgments

The research leading to these results is a contribution from the Projects PID2020-119412RJ-I00 of the Spanish Ministry of Science and Innovation to CG-L; "MarsFirstWater" (Consolidator Grant no. 818602), funded by the European Research Council, to AF; and PID2022-140180OB-C22 of the Spanish Ministry of Science and Innovation, to EM-M. We acknowledge S. Galvez-Martinez (PTA2021-019954-I) for his help and support during the XPS measurements.

Conflict of interest

The authors declare that the research was conducted in the absence of any commercial or financial relationships that could be construed as a potential conflict of interest.

The author(s) declared that they were an editorial board member of Frontiers, at the time of submission. This had no impact on the peer review process and the final decision.

Generative AI statement

The author(s) declare that no Generative AI was used in the creation of this manuscript.

Publisher's note

Supplementary material

The Supplementary Material for this article can be found online at: https://www.frontiersin.org/articles/10.3389/fspas.2025.1504288/full#supplementary-material

References

Amils, R., González-Toril, E., Fernández-Remolar, D., Gómez, F., Aguilera, Á., Rodríguez, N., et al. (2007). Extreme environments as Mars terrestrial analogs: the Rio Tinto case. *Planet. Space Sci.* 55 (3), 370–381. doi:10.1016/j.pss.2006.02.006

Baron, F., Gaudin, A., Lorand, J.-P., and Mangold, N. (2019). New constraints on early Mars weathering conditions from an experimental approach on crust simulants. *J. Geophys. Res. Planets* 124 (7), 1783–1801. doi:10.1029/2019je005920

Bishop, J. L., Fairén, A. G., Michalski, J. R., Gago-Duport, L., Baker, L. L., Velbel, M. A., et al. (2018). Surface clay formation during short-term warmer and wetter conditions on a largely cold ancient Mars. *Nat. Astron.* 2 (3), 206–213. doi:10.1038/s41550-017-0377-9

Bishop, J. L., King, S. J., Lane, M. D., Brown, A. J., Lafuente, B., Hiroi, T., et al. (2021). Spectral properties of anhydrous carbonates and nitrates. *Earth Space Sci.* 8 (10), e2021EA001844. doi:10.1029/2021ea001844

Bishop, J. L., Parente, M., Weitz, C. M., Noe Dobrea, E. Z., Roach, L. H., Murchie, S. L., et al. (2009). Mineralogy of Juventae Chasma: sulfates in the light-toned mounds, mafic minerals in the bedrock, and hydrated silica and hydroxylated ferric sulfate on the plateau. *J. Geophys. Res. Planets* 114 (E2). doi:10.1029/2009je003352

Borda, M. J., Elsetinow, A. R., Schoonen, M. A., and Strongin, D. R. (2001). Pyrite-induced hydrogen peroxide formation as a driving force in the evolution of photosynthetic organisms on an early earth. *Astrobiology* 1 (3), 283–288. doi:10.1089/15311070152757474

Burns, R. G. (1988). "Gossans on Mars," in *Proceedings of the 18th LPSC* (Houston, TX: LPI).

Burns, R. G. (1993). Rates and mechanisms of chemical weathering of ferromagnesian silicate minerals on Mars. *Geochim. Cosmochim. Acta* 57, 4555–4574. doi:10.1016/0016-7037(93)90182-v

Burns, R. G., and Fisher, D. S. (1990). Iron-sulfur mineralogy of Mars: magmatic evolution and chemical weathering products. *J. Geophys. Res. Solid Earth* 95 (B9), 14415–14421. doi:10.1029/jb095ib09p14415

Caro, G. M. M., Mateo-Martí, E., and Martínez-Frías, J. (2006). Near-UV transmittance of basalt dust as an analog of the martian regolith: implications for sensor calibration and astrobiology. *Sensors* 6 (6), 688–696. doi:10.3390/s6060688

Carrier, B. L., Abbey, W. J., Beegle, L. W., Bhartia, R., and Liu, Y. (2019). Attenuation of ultraviolet radiation in rocks and minerals: implications for Mars science. *J. Geophys. Res. Planets* 124 (10), 2599–2612. doi:10.1029/2018je005758

Changela, H. G., Chatzitheodoridis, E., Antunes, A., Beaty, D., Bouw, K., Bridges, J. C., et al. (2022). Mars: new insights and unresolved questions – corrigendum. *Int. J. Astrobiol.* 21 (1), 46. doi:10.1017/s1473550421000380

Chevrier, V., Lorand, J.-P., and Sautter, V. (2011). Sulfide petrology of four nakhlites: northwest africa 817, northwest africa 998, nakhla, and governador valadares. *Meteorit. and Planet. Sci.* 46 (6), 769–784. doi:10.1111/j.1945-5100.2011.01189.x

Chevrier, V., Mathé, P. E., Rochette, P., Grauby, O., Bourrié, G., and Trolard, F. (2006). Iron weathering products in a CO2+(H2O or H2O2) atmosphere: implications for weathering processes on the surface of Mars. *Geochimica Cosmochimica Acta* 70 (16), 4295–4317. doi:10.1016/j.gca.2006.06.1368

Chevrier, V., Rochette, P., Mathé, P.-E., and Grauby, O. (2004). Weathering of iron-rich phases in simulated Martian atmospheres. *Geology* 32 (12), 1033–1036. doi:10.1130/g21078.1

David, G., Dehouck, E., Meslin, P.-Y., Rapin, W., Cousin, A., Forni, O., et al. (2022). Evidence for amorphous sulfates as the main carrier of soil hydration in Gale Crater, Mars. *Geophys. Res. Lett.* 49 (21), e2022GL098755. doi:10.1029/2022gl098755

Dehouck, E., Chevrier, V., Gaudin, A., Mangold, N., Mathé, P. E., and Rochette, P. (2012). Evaluating the role of sulfide-weathering in the formation of sulfates or carbonates on Mars. *Geochimica Cosmochimica Acta* 90, 47–63. doi:10.1016/j.gca.2012.04.057

Dehouck, E., Gaudin, A., Chevrier, V., and Mangold, N. (2016). Mineralogical record of the redox conditions on early Mars. *Icarus* 271, 67–75. doi:10.1016/j.icarus.2016.01.030

Dehouck, E., Gaudin, A., Mangold, N., Lajaunie, L., Dauzères, A., Grauby, O., et al. (2014). Weathering of olivine under CO2 atmosphere: a martian perspective. *Geochimica Cosmochimica Acta* 135, 170–189. doi:10.1016/j.gca.2014.03.032

Delvigne, J., Bisdom, E. B. A., Sleeman, J., and Stoops, G. (1979). Olivines, their pseudomorphs and secondary products. *Pedologie* 29, 247–309.

Ding, S., Dasgupta, R., and Tsuno, K. (2014). Sulfur concentration of martian basalts at sulfide saturation at high pressures and temperatures – implications for deep sulfur cycle on Mars. *Geochimica Cosmochimica Acta* 131, 227–246. doi:10.1016/j.gca.2014.02.003

Eggleston, C., Stern, J., Strellis, T., and Parkinson, B. (2012). A natural photoelectrochemical cell for water splitting: implications for early Earth and Mars. *Am. Mineralogist* 97, 1804–1807. doi:10.2138/am.2012.4211

Ehlmann, B. L., Swayze, G. A., Milliken, R. E., Mustard, J. F., Clark, R. N., Murchie, S. L., et al. (2016). Discovery of alunite in Cross Crater, terra sirenum, Mars: evidence for acidic, sulfurous waters. *Am. Mineralogist* 101, 1527–1542. doi:10.2138/am-2016-5574

Ellerbrock, R., Stein, M., and Schaller, J. (2022). Comparing amorphous silica, short-range-ordered silicates and silicic acid species by FTIR. *Sci. Rep.* 12 (1), 11708. doi:10.1038/s41598-022-15882-4

Fairén, A. G. (2010). A cold and wet Mars. *Icarus* 208 (1), 165–175. doi:10.1016/j.icarus.2010.01.006

Fairén, A. G., Davila, A. F., Gago-Duport, L., Amils, R., and McKay, C. P. (2009). Stability against freezing of aqueous solutions on early Mars. *Nature* 459 (7245), 401–404. doi:10.1038/nature07978

Fairén, A. G., Davila, A. F., Gago-Duport, L., Haqq-Misra, J. D., Gil, C., McKay, C. P., et al. (2011). Cold glacial oceans would have inhibited phyllosilicate sedimentation on early Mars. *Nat. Geosci.* 4 (10), 667–670. doi:10.1038/ngeo1243

Fairén, A. G., Gil-Lozano, C., Uceda, E. R., Losa-Adams, E., Davila, A. F., and Gago-Duport, L. (2017). Mineral paragenesis on Mars: the roles of reactive surface area and diffusion. *J. Geophys. Res. Planets* 122 (9), 1855–1879. doi:10.1002/2016je005229

Fairley, N., Fernandez, V., Richard-Plouet, M., Guillot-Deudon, C., Walton, J., Smith, E., et al. (2021). Systematic and collaborative approach to problem solving using X-ray photoelectron spectroscopy. *Appl. Surf. Sci. Adv.* 5, 100112. doi:10.1016/j.apsadv.2021.100112

Feldman, A. D., Hausrath, E. M., Rampe, E. B., Tu, V., Peretyazhko, T. S., DeFelice, C., et al. (2024). Fe-rich X-ray amorphous material records past climate and persistence of water on Mars. *Commun. Earth and Environ.* 5 (1), 364. doi:10.1038/s43247-024-01495-4

Franz, H. B., King, P. L., and Gaillard, F. (2019). "Chapter 6 - sulfur on Mars from the atmosphere to the core," in *Volatiles in the martian crust*. Editors J. Filiberto, and S. P. Schwenzer (Elsevier), 119–183.

Gago-Duport, L., Briones, M. J. I., Rodríguez, J. B., and Covelo, B. (2008). Amorphous calcium carbonate biomineralization in the earthworm's calciferous gland: pathways to the formation of crystalline phases. *J. Struct. Biol.* 162 (3), 422–435. doi:10.1016/j.jsb.2008.02.007

Gaillard, F., and Scaillet, B. (2009). The sulfur content of volcanic gases on Mars. *Earth Planet. Sci. Lett.* 279 (1), 34–43. doi:10.1016/j.epsl.2008.12.028

Galvez-Martinez, S., Escamilla-Roa, E., Zorzano Mier, M.-P., and Mateo-Marti, E. (2019). Defects on a pyrite(100) surface produce chemical evolution of glycine under inert conditions: experimental and theoretical approaches. *Phys. Chem. Chem. Phys. - PCCP.* 21 (44), 24535–24542. doi:10.1039/c9cp03577j

Gil-Lozano, C., Baron, F., Gaudin, A., Lorand, J. P., Fernandez, V., Hamon, J., et al. (2024). The key role of bedrock composition in the formation of carbonates on Mars. *Geochem. Perspect. Lett.* 28, 54–59. doi:10.7185/geochemlet.2403

Gil-Lozano, C., Davila, A. F., Losa-Adams, E., Fairén, A. G., and Gago-Duport, L. (2017). Quantifying Fenton reaction pathways driven by self-generated H2O2 on pyrite surfaces. *Sci. Rep.* 7 (1), 43703. doi:10.1038/srep43703

Gil-Lozano, C., Losa-Adams, E., Dávila, A., and Gago-Duport, L. (2014). Pyrite nanoparticles as a Fenton-like reagent for *in situ* remediation of organic pollutants. *Beilstein J. Nanotechnol.* 5, 855–864. doi:10.3762/bjnano.5.97

Góbi, S., and Kereszturi, Á. (2019). Analyzing the role of interfacial water on sulfate formation on present Mars. *Icarus* 322, 135–143. doi:10.1016/j.icarus.2019.01.005

Gómez-Elvira, J., Armiens, C., Carrasco, I., Genzer, M., Gómez, F., Haberle, R., et al. (2014). Curiosity's rover environmental monitoring station: overview of the first 100 sols. *J. Geophys. Res. Planets* 119 (7), 1680–1688. doi:10.1002/2013je004576

Grosvenor, A. P., Kobe, B. A., Biesinger, M. C., and McIntyre, N. S. (2004). Investigation of multiplet splitting of Fe 2p XPS spectra and bonding in iron compounds. *Surf. Interface Analysis* 36 (12), 1564–1574. doi:10.1002/sia.1984

Herbert, F. W., Krishnamoorthy, A., Van Vliet, K. J., and Yildiz, B. (2013). Quantification of electronic band gap and surface states on FeS2(100). *Surf. Sci.* 618, 53–61. doi:10.1016/j.susc.2013.08.014

Hewins, R. H., Zanda, B., Humayun, M., Nemchin, A., Lorand, J.-P., Pont, S., et al. (2017). Regolith breccia northwest africa 7533: mineralogy and petrology with implications for early Mars. *Meteorit. and Planet. Sci.* 52 (1), 89–124. doi:10.1111/maps.12740

Jakosky, B. M., Brain, D., Chaffin, M., Curry, S., Deighan, J., Grebowsky, J., et al. (2018). Loss of the Martian atmosphere to space: present-day loss rates determined from MAVEN observations and integrated loss through time. *Icarus* 315, 146–157. doi:10.1016/j.icarus.2018.05.030

Javadi Nooshabadi, A., and Hanumantha Rao, K. (2014). Formation of hydrogen peroxide by sulphide minerals. *Hydrometallurgy* 141, 82–88. doi:10.1016/j.hydromet.2013.10.011

Jiang, C. Z., and Tosca, N. J. (2020). Growth kinetics of siderite at 298.15 K and 1 bar. *Geochimica Cosmochimica Acta* 274, 97–117. doi:10.1016/j.gca.2020.01.047

Kwak, J. H., Hu, J. Z., Turcu, R. V. F., Rosso, K. M., Ilton, E. S., Wang, C., et al. (2011). The role of H2O in the carbonation of forsterite in supercritical CO2. *Int. J. Greenh. Gas Control* 5 (4), 1081–1092. doi:10.1016/j.ijggc.2011.05.013

Lane, M. D. (2007). Mid-infrared emission spectroscopy of sulfate and sulfate-bearing minerals. *Am. Mineralogist* 92 (1), 1–18. doi:10.2138/am.2007.2170

Lasaga, A. C. (1998). *Kinetic theory in the Earth Sciences*. Princeton University Press.

Lasne, J., Noblet, A., Szopa, C., Navarro-González, R., Cabane, M., Poch, O., et al. (2016). Oxidants at the surface of Mars: a review in light of recent exploration results. *Astrobiology* 16 (12), 977–996. doi:10.1089/ast.2016.1502

Lorand, J.-P., Hewins, R. H., Remusat, L., Zanda, B., Pont, S., Leroux, H., et al. (2015). Nickeliferous pyrite tracks pervasive hydrothermal alteration in Martian regolith breccia: a study in NWA 7533. *Meteorit. and Planet. Sci.* 50 (12), 2099–2120. doi:10.1111/maps.12565

Lorand, J.-P., Pont, S., Chevrier, V., Luguet, A., Zanda, B., and Hewins, R. (2018). Petrogenesis of martian sulfides in the Chassigny meteorite. *Am. Mineralogist* 103 (6), 872–885. doi:10.2138/am-2018-6334

Macey, M. C., Fox-Powell, M., Ramkissoon, N. K., Stephens, B. P., Barton, T., Schwenzer, S. P., et al. (2020). The identification of sulfide oxidation as a potential metabolism driving primary production on late Noachian Mars. *Sci. Rep.* 10 (1), 10941. doi:10.1038/s41598-020-67815-8

Mateo-Marti, E., Galvez-Martinez, S., Gil-Lozano, C., and Zorzano, M.-P. (2019). Pyrite-induced uv-photocatalytic abiotic nitrogen fixation: implications for early atmospheres and Life. *Sci. Rep.* 9 (1), 15311. doi:10.1038/s41598-019-51784-8

Mateo-Martí, E., Prieto-Ballesteros, O., Sobrado, J. M., Gómez-Elvira, J., and Martín-Gago, J. A. (2006). A chamber for studying planetary environments and its applications to astrobiology. *Meas. Sci. Technol.* 17 (8), 2274–2280. doi:10.1088/0957-0233/17/8/031

McAdam, A. C., Franz, H. B., Sutter, B., Archer, Jr. P. D., Freissinet, C., Eigenbrode, J. L., et al. (2014). Sulfur-bearing phases detected by evolved gas analysis of the Rocknest aeolian deposit, Gale Crater, Mars. *J. Geophys. Res. Planets* 119 (2), 373–393. doi:10.1002/2013je004518

McCubbin, F. M., Tosca, N. J., Smirnov, A., Nekvasil, H., Steele, A., Fries, M., et al. (2009). Hydrothermal jarosite and hematite in a pyroxene-hosted melt inclusion in martian meteorite Miller Range (MIL) 03346: implications for magmatic-hydrothermal fluids on Mars. *Geochimica Cosmochimica Acta* 73 (16), 4907–4917. doi:10.1016/j.gca.2009.05.031

McKibben, M. A., and Barnes, H. L. (1986). Oxidation of pyrite in low temperature acidic solutions: rate laws and surface textures. *Geochimica Cosmochimica Acta* 50 (7), 1509–1520. doi:10.1016/0016-7037(86)90325-x

Mitra, K., Catalano, J. G., Bahl, Y., and Hurowitz, J. A. (2023). Iron sulfide weathering by oxyhalogen species: implications for iron sulfate and (oxyhydr)oxides formation on Mars. *Earth Planet. Sci. Lett.* 624, 118464. doi:10.1016/j.epsl.2023.118464

Moore, R. D., and Szynkiewicz, A. (2023). Aqueous sulfate contributions in terrestrial basaltic catchments: implications for understanding sulfate sources and transport in Meridiani Planum, Mars. *Icarus* 391, 115342. doi:10.1016/j.icarus.2022.115342

Mukhin, L. M., Koscheevi, A. P., Dikov, Y. P., Huth, J., and Wänke, H. (1996). Experimental simulations of the photodecomposition of carbonates and sulphates on Mars. *Nature* 379 (6561), 141–143. doi:10.1038/379141a0

Nachon, M., Clegg, S. M., Mangold, N., Schröder, S., Kah, L. C., Dromart, G., et al. (2014). Calcium sulfate veins characterized by ChemCam/Curiosity at Gale crater, Mars. *J. Geophys. Res. Planets* 119 (9), 1991–2016. doi:10.1002/2013je004588

Palandri, J. L., and Kharaka, Y. K. (2004). A compilation of rate parameters of water-mineral interaction kinetics for application to geochemical modeling. *Report*, 2004–1068. doi:10.3133/ofr20041068

Parkhurst, D. L., and Appelo, C. A. J. (2013). Description of input and examples for PHREEQC version 3: a computer program for speciation, batch-reaction, one-dimensional transport, and inverse geochemical calculations. *Report*, 6–A43. doi:10.3133/tm6A43

Patel, M. R., Bérces, A., Kerékgyárto, T., Rontó, G., Lammer, H., and Zarnecki, J. C. (2004). Annual solar UV exposure and biological effective dose rates on the Martian surface. *Adv. Space Res.* 33 (8), 1247–1252. doi:10.1016/j.asr.2003.08.036

Peak, D., Ford, R. G., and Sparks, D. L. (1999). An *in situ* ATR-FTIR investigation of sulfate bonding mechanisms on goethite. *J. Colloid Interface Sci.* 218 (1), 289–299. doi:10.1006/jcis.1999.6405

Peretyazhko, T. S., Ming, D. W., Morris, R. V., Agresti, D. G., and Buckley, W. P. (2021). Formation of Fe(III) (Hydr)oxides from Fe(II) sulfides: implications

for akaganeite detection on Mars. *ACS Earth Space Chem.* 5 (8), 1934–1947. doi:10.1021/acsearthspacechem.1c00075

Quinn, R., Zent, A. P., and McKay, C. P. (2006). The photochemical stability of carbonates on Mars. *Astrobiology* 6 (4), 581–591. doi:10.1089/ast.2006.6.581

Ramkissoon, N. K., Pearson, V. K., Schwenzer, S. P., Schröder, C., Kirnbauer, T., Wood, D., et al. (2019). New simulants for martian regolith: controlling iron variability. *Planet. Space Sci.* 179, 104722. doi:10.1016/j.pss.2019.104722

Rampe, E. B., Blake, D. F., Bristow, T. F., Ming, D. W., Vaniman, D. T., Morris, R. V., et al. (2020). Mineralogy and geochemistry of sedimentary rocks and eolian sediments in Gale crater, Mars: a review after six Earth years of exploration with Curiosity. *Geochemistry* 80 (2), 125605. doi:10.1016/j.chemer.2020.125605

Roisnel, T., and Rodriguez-Carvajal, J. (2001). WinPLOTR: a Windows tool for powder diffraction pattern analysis. *Mater. Sci. Forum* 378, 118–123. doi:10.4028/www.scientific.net/MSF.378-381.118

Schaufuß, A. G., Nesbitt, H. W., Kartio, I., Laajalehto, K., Bancroft, G. M., and Szargan, R. (1998). Incipient oxidation of fractured pyrite surfaces in air. *J. Electron Spectrosc. Relat. Phenom.* 96 (1), 69–82. doi:10.1016/s0368-2048(98)00237-0

Schoonen, M., Elsetinow, A., Borda, M., and Strongin, D. (2000). Effect of temperature and illumination on pyrite oxidation between pH 2 and 6. *Geochem. Trans.* 1 (1), 23. doi:10.1186/1467-4866-1-23

Schuttlefield, J. D., Sambur, J. B., Gelwicks, M., Eggleston, C. M., and Parkinson, B. A. (2011). Photooxidation of chloride by oxide minerals: implications for perchlorate on Mars. *J. Am. Chem. Soc.* 133 (44), 17521–17523. doi:10.1021/ja2064878

Schwenzer, S. P., Bridges, J. C., Wiens, R. C., Conrad, P. G., Kelley, S. P., Leveille, R., et al. (2016). Fluids during diagenesis and sulfate vein formation in sediments at Gale crater, Mars. *Meteorit. and Planet. Sci.* 51 (11), 2175–2202. doi:10.1111/maps.12668

Shidare, M., Nakada, R., Usui, T., Tobita, M., Shimizu, K., Takahashi, Y., et al. (2021). Survey of impact glasses in shergottites searching for Martian sulfate using X-ray absorption near-edge structure. *Geochimica Cosmochimica Acta* 313, 85–98. doi:10.1016/j.gca.2021.08.026

Sonnenthal, E., Ito, A., Spycher, N., Yui, M., Apps, J., Sugita, Y., et al. (2005). Approaches to modeling coupled thermal, hydrological, and chemical processes in the drift scale heater test at Yucca Mountain. *Int. J. Rock Mech. Min. Sci.* 42 (5), 698–719. doi:10.1016/j.ijrmms.2005.03.009

Sweetman, A. K., Smith, A. J., de Jonge, D. S. W., Hahn, T., Schroedl, P., Silverstein, M., et al. (2024). Evidence of dark oxygen production at the abyssal seafloor. *Nat. Geosci.* 17 (8), 737–739. doi:10.1038/s41561-024-01480-8

Tang, X., Tang, R., Xiong, S., Zheng, J., Li, L., Zhou, Z., et al. (2022). Application of natural minerals in photocatalytic degradation of organic pollutants: a review. *Sci. total Environ.* 812, 152434. doi:10.1016/j.scitotenv.2021.152434

Thorpe, M. T., Bristow, T. F., Rampe, E. B., Tosca, N. J., Grotzinger, J. P., Bennett, K. A., et al. (2022). Mars science laboratory CheMin data from the glen Torridon region and the significance of lake-groundwater interactions in interpreting mineralogy and sedimentary history. *J. Geophys. Res. Planets* 127 (11), e2021JE007099. doi:10.1029/2021je007099

Todd, E. C., Sherman, D. M., and Purton, J. A. (2003). Surface oxidation of pyrite under ambient atmospheric and aqueous (pH = 2 to 10) conditions: electronic structure and mineralogy from X-ray absorption spectroscopy. *Geochimica Cosmochimica Acta* 67 (5), 881–893. doi:10.1016/s0016-7037(02)00957-2

Vaniman, D. T., Bish, D. L., Ming, D. W., Bristow, T. F., Morris, R. V., Blake, D. F., et al. (2014). Mineralogy of a mudstone at Yellowknife Bay, Gale crater, Mars. *Sci. (New York, NY)* 343 (6169), 1243480. doi:10.1126/science.1243480

Wang, W., Qu, Y., Yang, B., Liu, X., and Su, W. (2012). Lactate oxidation in pyrite suspension: a Fenton-like process *in situ* generating H2O2. *Chemosphere* 86 (4), 376–382. doi:10.1016/j.chemosphere.2011.10.026

Weitz, C. M., Bishop, J. L., Thollot, P., Mangold, N., and Roach, L. H. (2011). Diverse mineralogies in two troughs of Noctis Labyrinthus, Mars. *Geology* 39 (10), 899–902. doi:10.1130/g32045.1

Wittmann, A., Korotev, R. L., Jolliff, B. L., Irving, A. J., Moser, D. E., Barker, I., et al. (2015). Petrography and composition of Martian regolith breccia meteorite Northwest Africa 7475. *Meteorit. and Planet. Sci.* 50 (2), 326–352. doi:10.1111/maps.12425

Wong, G. M., Franz, H. B., Clark, J. V., McAdam, A. C., Lewis, J. M. T., Millan, M., et al. (2022). Oxidized and reduced sulfur observed by the sample analysis at Mars (SAM) instrument suite on the curiosity rover within the glen Torridon region at Gale Crater, Mars. *J. Geophys. Res. Planets* 127 (9), e2021JE007084. doi:10.1029/2021je007084

Wray, J. J., Milliken, R. E., Dundas, C. M., Swayze, G. A., Andrews-Hanna, J. C., Baldridge, A. M., et al. (2011). Columbus crater and other possible groundwater-fed paleolakes of Terra Sirenum, Mars. *J. Geophys. Res. Planets* 116 (E1), E01001. doi:10.1029/2010je003694

Wray, J. J., Squyres, S. W., Roach, L. H., Bishop, J. L., Mustard, J. F., and Noe Dobrea, E. Z. (2010). Identification of the Ca-sulfate bassanite in Mawrth Vallis, Mars. *Icarus* 209 (2), 416–421. doi:10.1016/j.icarus.2010.06.001

Xian, H., Zhu, J., Tan, W., Tang, H., Liu, P., Zhu, R., et al. (2019). The mechanism of defect induced hydroxylation on pyrite surfaces and implications for hydroxyl radical generation in prebiotic chemistry. *Geochimica Cosmochimica Acta* 244, 163–172. doi:10.1016/j.gca.2018.10.009

Zhang, P., Yuan, S., and Liao, P. (2016). Mechanisms of hydroxyl radical production from abiotic oxidation of pyrite under acidic conditions. *Geochimica Cosmochimica Acta* 172, 444–457. doi:10.1016/j.gca.2015.10.015

Zhang, Y., Hu, B., Teng, Y., Tu, K., and Zhu, C. (2019). A library of BASIC scripts of reaction rates for geochemical modeling using phreeqc. *Comput. and Geosciences* 133, 104316. doi:10.1016/j.cageo.2019.104316

Zhu, P., Chen, Y., Duan, M., Liu, M., and Zou, P. (2018). Structure and properties of Ag3PO4/diatomite photocatalysts for the degradation of organic dyes under visible light irradiation. *Powder Technol.* 336, 230–239. doi:10.1016/j.powtec.2018.05.060

Zolotov, M. Y., and Mironenko, M. V. (2016). Chemical models for martian weathering profiles: insights into formation of layered phyllosilicate and sulfate deposits. *Icarus* 275, 203–220. doi:10.1016/j.icarus.2016.04.011